Synthesis, Structural, and Transport Properties of Novel Bihydrated Fluorosulphates NaMSO4F center dot 2H(2)O (M = Fe, Co, and Ni)

ARTICLE *in* CHEMISTRY OF MATERIALS · JULY 2010

Impact Factor: 8.35 · DOI: 10.1021/cm1010482

4062 *Chem. Mater.* **2010,** *22,* 4062–4068
DOI:10.1021/cm1010482

CHEMISTRY OF MATERIALS
Article

Synthesis, Structural, and Transport Properties of Novel Bihydrated Fluorosulphates $NaMSO_4F \cdot 2H_2O$ (M = Fe, Co, and Ni)

M. Ati,[†] L. Dupont,[†] N. Recham,[†] J.N. Chotard,[†] W.T. Walker,[†] C. Davoisne,[†] P. Barpanda,[†] V. Sarou-Kanian,[‡] M. Armand,[†] and J.M. Tarascon*[,†]

[†]*LRCS, CNRS-UMR 6007, Université de Picardie Jules Verne, 33 rue Saint Leu, 80039 Amiens, France, and* [‡]*CEMHTI, CNRS-UPR 3079, 1D, Avenue de la Recherche Scientifique, 45071 Orléans, France*

Received April 15, 2010. Revised Manuscript Received May 31, 2010

3*d*-metal fluorosulphates that have a tavorite-type structure (e.g., $LiFeSO_4F$) were recently reported as attractive positive electrode candidates for future Li-ion batteries aimed at large volume markets. These new fluorosulphates had to be synthesized via ionothermal synthesis owing to both their thermal instability at temperatures greater than 300 °C and their water solubility. In an attempt to depart from ionothermal synthesis, low-temperature solid-state reactions and solvothermal processes were successfully tried. The latter technique, which is reported herein, proceeds with water as the solvent and has led to a new family of fluorosulphates $NaMSO_4F \cdot 2H_2O$ that crystallize in a monoclinic unit cell (SG = $P2_1/m$) similar to the uklonskovite-type structure earlier proposed for $NaMgSO_4F \cdot 2H_2O$. These new phases show no electrochemical activity with either Li or Na metal and have room temperature ionic conductivities on the order of 1×10^{-9} S cm^{-1}. Additionally, we have discovered the feasibility, upon controlled dehydration of the $NaMSO_4F.2H_2O$ phases, to prepare $NaMSO_4F$ phases adopting a derived tavorite-type structure and displaying ionic conductivities around 10^{-7} S cm^{-1}. Finally, this finding opens the possibility to achieve Li-based fluorosulphates via two-step synthetic pathways.

Introduction

Because of the economical and societal impact with respect to energy storage, Li-ion technology has, over the past decade, challenged the research community generally and more specifically the solid-state chemists to design better inorganic positive electrodes.[1,2] The journey of Li-based insertion materials research, which started more than two decades ago with lamellar ($LiMO_2$; M = Co, Ni) and three-dimensional ($LiMn_2O_4$) electrodes, has recently led to the development of a wide range of oxygen-based polyanionic compounds having M−O bonding such as olivines ($LiMPO_4$, M = Fe, Mn, Co, Ni), borates, silicates, etc.[3−5] These materials, owing to the inductive effect associated with the replacement of O^{2-} by polyanionic species such as $(PO_4)^{3-}$, $(BO_3)^{3-}$, $(SiO_4)^{4-}$, generally show higher insertion voltages for the same M^{n+}/M^{n+1} redox couple than their corresponding 3d-metal oxides.[6,7] Furthermore, building on the inductive effect, it should be noted that the isostructural replacement of $(PO_4)^{3-}$ with $(SO_4)^{2-}$ in Fe-based NASICON-type structures improves the redox voltage by 800 mV because of the inductive effect.[8] Additionally, the introduction of fluorine can improve the open circuit voltage (and redox potential) of these systems because of the larger ionicity of M−F bonding compared to M−O bonding. Indeed, many fluorine-based compounds have recently been developed to propel the next generation Li-ion batteries. Following Barker's pioneering work on F-based electrodes,[9,10] we have successfully reported various fluorophosphates ($LiFePO_4F$, $LiTiPO_4F$, Na_2FePO_4F, etc.) having excellent electrochemical activity and rate-capability.[11−13]

We have successfully combined the positive voltage attributes of both $(SO_4)^{2-}$ polyanions and F^- anions in a single compound via ionothermal synthesis to generate a novel fluorosulphate electrode, $LiFeSO_4F$, with excellent capacity (140 mA h/g), rate capability and cycling stability with a 3.6 V Fe^{II}/Fe^{III} redox reaction.[14] In addition to the use of ionic liquids, the use a iron sulfate monohydrate

*Corresponding author. E-mail: jean-marie.tarascon@sc.u-picardie.fr.

(1) Armand, M.; Tarascon, J.-M. *Nature* **2008**, *451*, 652–657.
(2) Tarascon, J.-M.; Armand, M. *Nature* **2001**, *414*, 359–367.
(3) Mizushima, K.; Jones, P. C.; Wiseman, P. C.; Goodenough, J. B. *Mater. Res. Bull.* **1980**, *15*(6), 783–789.
(4) Tarascon, J.-M.; Guyomard, D. *Solid State Ionics* **1994**, *69*, 222–237.
(5) Padhi, A. K.; Nanjundaswamy, K. S.; Goodenough, J. B. *J. Electrochem. Soc.* **1997**, *144*(4), 1188–1194.
(6) Legagneur, V.; An, Y.; Mosbah, A.; Portal, R.; Salle, A.; Verbaere, A.; Guyomard, D.; Piffard, Y. *Solid State Ionics.* **2001**, *139*, 37–46.
(7) Nytén, A.; Abouimrane, A.; Armand, M.; Gustafsson, T.; Thomas, J. O. *Electrochem. Commun.* **2005**, *7*(2), 156–160.
(8) Padhi, A. K.; Nanjundaswamy, K. S.; Masquelier, C.; Goodenough, J. B. *J. Electrochem. Soc.* **1997**, *144*, 2581–2586.
(9) Barker, J.; Saidi, M. Y.; Swoyer, J. L. *J. Electrochem. Soc.* **2003**, *150*, A1394–A1398.
(10) Barker, J.; Saidi, M. Y.; Swoyer, J. L. International Patent WO0184655.
(11) Recham, N.; Chotard, J.-N.; Jumas, J.-C.; Laffont, L.; Armand, M.; Tarascon, J.-M. *Chem. Mater.* **2010**, *22*(3), 1142–1148.
(12) Recham, N.; Chotard, J.-N.; Dupont, L.; Djellab, K.; Armand, M.; Tarascon, J.-M. *J. Electrochem. Soc.* **2009**, *156*, A993–A999.
(13) Tarascon, J.-M.; Recham, N.; Armand, M.; Chotard, J.-N.; Barpanda, P.; Walker, W.; Dupont, L. *Chem. Mater.* **2010**, *22*, 724–739.
(14) Recham, N.; Chotard, J.-N.; Dupont, L.; Delacourt, C.; Walker, W.; Armand, M.; Tarascon, J.-M. *Nat. Mater.* **2010**, *9*(1), 68–75.

 Published on Web 06/15/2010

precursor phase ($FeSO_4 \cdot H_2O$) is essential in the preparation of $LiFeSO_4F$ from LiF, because this reaction has been shown to be topotactic with the replacement of O^{2-} from H_2O by F^- in $FeSO_4 \cdot H_2O$ together with the ingress of one Li^+ for charge compensation.[13,14] Capitalizing on this topotactic reaction mechanism, a wide variety of tavorite-structured fluorosulphate derivatives such as $AMSO_4F$ and $A(Fe_{1-x}M_x)SO_4F$ (A = Li, Na and M = Fe, Co, Ni) have been discovered.[15,16] Such novel phases were shown to both decompose at temperatures greater than 350 °C and to be water-soluble, providing insight as to why previous attempts to prepare such phases by either ceramic methods or low-temperature synthetic approaches in aqueous media have failed.[13,14]

Sulphates are known for their water solubility because, in solution, M−O bonds are equally likely to form with either H_2O or $(SO_4)^{2-}$, as the bonding valences for the oxygen within these two species is ~0.17 v.u (for simple comparison, $(PO_4)^{3-}$ species are less soluble in water because of their greater oxygen bond valences (~0.25 v.u)). So, in light of such considerations, the water solubility of the new $AMSO_4F$ sulphates did not come as a surprise. In contrast, the reported existence of $NaMgSO_4F \cdot 2H_2O$,[17] a derived version of the water-soluble $NaMgSO_4F$ phase, was somewhat intriguing, although it should be noted that the size and electropositivity of the cations can perturb the oxygen bonding strength (for instance, O−H has a valence unit that can vary from 0.75 to 0.85), hence the feasibility of tuning the water solubility of sulphates. On the basis of these considerations, we herein report the synthesis, structural characteristics, and transport properties of novel bihydrated fluorosulphates ($NaMSO_4F \cdot 2H_2O$).

Results

Synthesis. Several procedures were used to prepare the $NaMSO_4F.nH_2O$ depending upon the nature of M. For M = Co and Ni, the reaction simply consisted of: (i) separately dissolving stoichiometric amounts of the corresponding hydrated phase ($MSO_4 \cdot nH_2O$ regardless of n) and NaF in enough water to obtain transparent, fully dissolved solutions; (ii) combining the two solutions; (iii) heating at 80 °C under stirring (~5 h) until ~90% of the water evaporated; and (iv) precipitating the remaining in a large excess of ethanol and collecting the product by centrifugation and drying at 100 °C in air for 1 h. A similar procedure was used for M= Fe, with the difference being that special care was taken in the experimental setup to prevent oxidation. Specifically, in a two-neck round-bottom flask fitted with a distillation setup, stoichiometric amounts of $FeSO_4 \cdot nH_2O$ and NaF were combined under nitrogen. Next, enough degassed water was added to dissolve the starting materials and the reaction mixture was heated to 100 °C until 90% of the water was removed. The remaining solution was removed via syringe and the product precipitated in a round-bottom flask under nitrogen containing degassed ethanol. Finally, excess ethanol was decanted and the solid was quickly transferred to a vacuum line so as to limit exposure to oxygen.

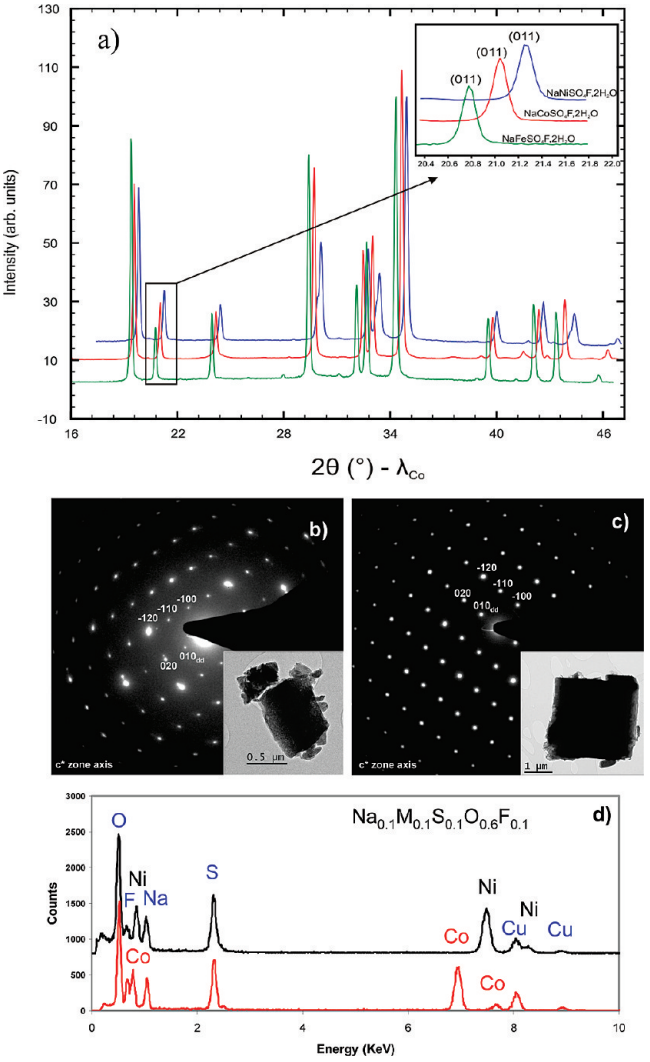

Figure 1. (a) X-ray powder patterns of the $NaMSO_4F \cdot 2H_2O$ phases (reprecipitated in ethanol); inset, the shift in the Bragg peak position as Fe is successively replaced by Co and Ni. (b, c) TEM study realized on nickel and cobalt hydrated sodium fluorosulphates within the characteristic SAED patterns collected along the c^* zone axis; insets, image of the particle for nickel and cobalt phases, respectively. (d) Corresponding EDS spectra leading to a composition consistent with the twice-hydrated fluorosulphate.

The above conditions led to powders that ranged in color from white, pink to green depending on the metal used (i.e., M = Fe, Co, and Ni). However, XRD analysis resulted in powder patterns that were very similar (Figure 1a) suggesting single-phased materials. The only difference in XRD patterns is a slight shift (Figure 1a inset) of the Bragg peaks, which is expected when dealing with 3d metal ions of different sizes. In contrast, the appearance of extra Bragg peaks, suggesting multiphased samples, was noted when the powders were recovered after complete water evaporation.

Structure. To determine the crystallographic structures of the obtained homologues of transition metal (Fe, Co, Ni)

(15) Barpanda, P.; Recham, N.; Chotard, J.-N.; Djellab, K.; Walker, W.; Armand, M.; Tarascon, J.-M. *J. Mater. Chem.* **2010**, *20*(9), 1659–1668.
(16) Barpanda, P.; Chotard, J.-N.; Recham, N.; Delacourt, C.; Ati, M.; Dupont, L.; Armand, M.; Tarascon, J.-M. Inorg. Chem. Submitted.
(17) Sabelli, C. *Bull. Mineral.* **1985**, *108*, 133–138.

sodium fluorosulphate bihydrates, we performed TEM studies using a FEI Tecnai F20 S-Twin electron microscope operating at 200 kV and fitted with an EDAX energy-dispersive spectrometer (EDS). The TEM results for the Co and Ni samples are the only results reported here in an attempt to avoid redundancy, as all samples were alike regardless of which 3d metal was utilized. Their powders consist of micrometric particles having a pseudo cubic shape. For each particle, a selected area electron diffraction study was realized in order to be able to draw the reciprocal space and an associated energy-dispersive spectroscopy spectrum was recorded to determine the chemical composition. Thus, from the electron crystallography work, a monoclinic cell having the following average parameters was proposed for the two samples: a = 5.7 Å, b = 7.3 Å, c = 7.2 Å, β = 114°. Moreover, only one condition ($0k0$ k = $2n$) limiting the possible reflections was recorded when the double diffraction phenomenon was not possible. For both nickel and cobalt phases, a representative SAED pattern recorded along the c*zone axis is given as an example in parts b and c in Figure 1, respectively. From the EDS spectra collected on both Ni- and Co-based particles (Figure 1d), we concluded their elemental makeup to be roughly Na, 10%; M, 10%; S, 10%; F, 10%; O, 60%. On the basis of the expected formula for a fluorosulphate, an excess of 2 oxygens is measured. Such extra oxygen could indicate the presence of water within the structure and therefore explain the instability of the samples when exposed to an intense electron beam while conducting TEM studies. Combining both chemical and crystallographic information with the JCPDS database, it could be proposed that the novel Fe, Co and Ni structure were isostructural to the Uklonskovite-type $NaMgSO_4F\cdot 2H_2O$ structure[17] (a = 7.202 Å, b = 7.214 Å, c = 5.734 Å, β = 113.23°, S.G. = $P2_1/m$).

On the basis of these findings, full structure refinements were realized from the powder XRD patterns. The X-ray diffraction studies were conducted using a Bruker D8 Diffractometer with Co Kα radiation (λ_1 = 1.7892 Å, λ_2 = 1.7932 Å) equipped with a Vantec detector. For the three samples (M = Ni, Co, and Fe), the powder patterns were indexed using DICVOL[18] and the Uklonskovite-type structure was confirmed. The structures were further refined using the FullProf program[19] (see Figure 2a), starting with atomic coordinates found by FOX.[20] The resulting standardized refined cell parameters are a = 5.73364(2) Å, b = 7.314981(17) Å, c = 7.18640(2) Å, β = 113.5028(2)°, SG = $P2_1/m$ for $NaCoSO_4F\cdot 2H_2O$; a = 5.70118(4) Å, b = 7.27603(3) Å, c = 7.15634(3) Å, β = 113.8883(2)°, SG = $P2_1/m$ for $NaNiSO_4F\cdot 2H_2O$; and a = 5.75959(5) Å, b = 7.38273(5) Å, c = 7.250447(7) Å, β = 113.3225(6), SG = $P2_1/m$ for $NaFeSO_4F\cdot 2H_2O$. The complete structural data are summarized in Tables 1 and 2 and the refined powder pattern of $NaCoSO_4F\cdot 2H_2O$ is presented in Figure 2a. Needless to say that such a structural model was established by analogy with that of $NaMgSO_4F\cdot 2H_2O$, because distinguishing between O, F, and OH_2 is not an easy task from X-ray powder diffraction.

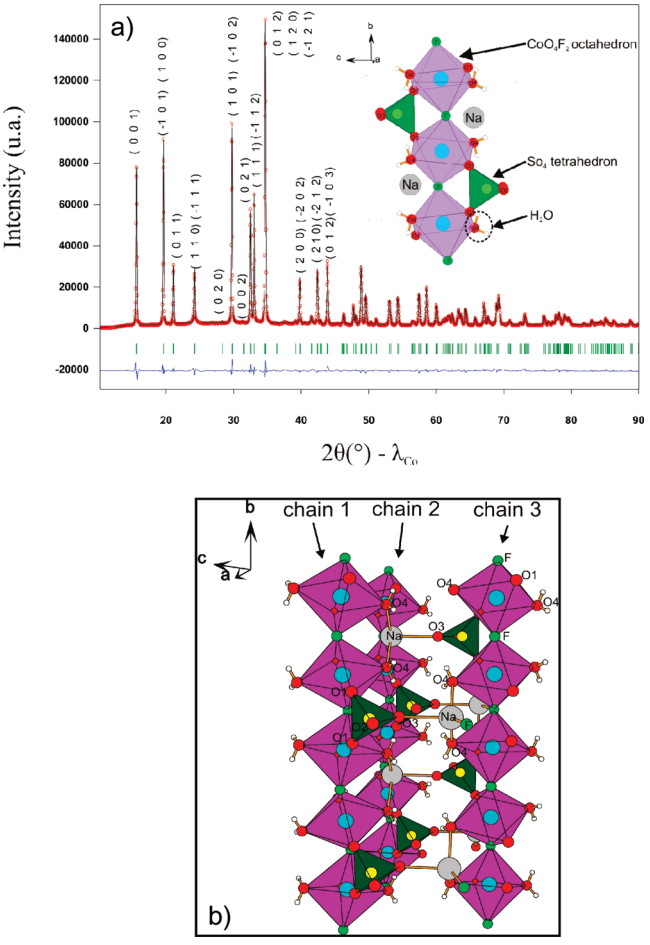

Figure 2. (a) Rietveld refinement results for the $NaCoSO_4F.2H_2O$ phase. Red open circle represents the observed data points and the black line presents the calculated pattern. The difference pattern is plotted in blue, whereas the calculated reflections are plotted with green ticks. The projection along the a axis of the $NaMSO_4F\cdot 2H_2O$ structure is shown as the inset. MO_4F_2 octahedra are depicted in purple, whereas SO_4 tetrahedrons are in green. Large gray spheres and small white spheres represent sodium and hydrogen respectively. (b) View of the interconnected chains in $NaCoSO_4F\cdot 2H_2O$ showing the interconnections of the MO_4F_2/SO_4.

Table 1. Crystal Data and Rietveld Refinement Parameters for $NaFeSO_4F\cdot 2H_2O$, $NaCoSO_4F\cdot 2H_2O$, and $NaNiSO_4F\cdot 2H_2O$

	$NaFeSO_4F\cdot 2H_2O$	$NaCoSO_4F\cdot 2H_2O$	$NaNiSO_4F\cdot 2H_2O$
space group	$P2_1/m$	$P2_1/m$	$P2_1/m$
a (Å)	5.75959(5)	5.73364(2)	5.70118(4)
b (Å)	7.38273(5)	7.314981(17)	7.27603(3)
c (Å)	7.250447(7)	7.18640(2)	7.15634(3)
β (deg)	113.3225(6)	113.5028(2)	113.8883(2)
V (Å^3)	283.109(11)	276.40(9)	271.429(15)
agreement factors χ^2	7.08	24.1	23.8
R_p	11.9	8.48	7.15
R_{wp}	11.6	9.93	5.92
R_{Bragg}	6.49	3.63	2.45

For the three compounds, the structure is built from 3d metal centered MO_4F_2 octahedrons linked together with F atoms in trans position. Among the 4 oxygen atoms constituting the equatorial plain of those octahedrons, two (labeled O4) are from an H_2O molecule, whereas the

(18) Boultif, A.; Louer, D. *J. Appl. Crystallogr.* **2004**, *37*, 724–731.
(19) Rodríguez-Carvajal, J. *Physica B* **1993**, *192*, 55–69.
(20) Favre-Nicolin, V.; Cerny, R. *J. Appl. Crystallogr.* **2002**, *35*, 734–743.

Table 2. Atomic Coordinates of $NaCoSO_4F \cdot 2H_2O$, $NaNiSO_4F \cdot 2H_2O$, and $NaFeSO_4F \cdot 2H_2O$

atom	Wyckoff position	*x*	*y*	*z*	occupation
		$NaCoSO_4F \cdot 2H_2O$			
Na	2*e*	0.1212(12)	1/4	0.6992(7)	1
Co	2*d*	1/2	0	1/2	1
F	2*e*	0.3700(10)	1/4	0.5196(11)	1
S	2*e*	0.6496(9)	1/4	0.1911(6)	1
O1	4*f*	0.7030(9)	0.0892(8)	0.3208(7)	1
O2	2*e*	0.8293(16)	1/4	0.0844(13)	1
O3	2*e*	0.3798(16)	1/4	0.0466(12)	1
H1	4*f*	0.20500	0.58200	0.15400	1
H2	4*f*	0.09200	0.04500	0.20400	1
O4	4*f*	0.1596(10)	0.5446(6)	0.2368(8)	1
		$NaNiSO_4F \cdot 2H_2O$			
Na	2*e*	0.1184(10)	1/4	0.6916(8)	1
Ni	2*d*	1/2	0	1/2	1
F	2*e*	0.3673(10)	1/4	0.5195(9)	1
S	2*e*	0.6411(9)	1/4	0.1917(10)	1
O1	4*f*	0.7089(8)	0.0902(10)	0.3296(8)	1
O2	2*e*	0.8338(17)	1/4	0.0921(11)	1
O3	2*e*	0.3727(19)	1/4	0.0458(11)	1
H1	4*f*	0.20500	0.58200	0.15400	1
H2	4*f*	0.09200	0.04500	0.20400	1
O4	4*f*	0.1726(9)	0.5434(6)	0.2403(7)	1
		$NaFeSO_4F \cdot 2H_2O$			
Na	2*e*	0.1294(13)	1/4	0.7066(8)	1
Fe	2*d*	1/2	0	1/2	1
F	2*e*	0.3917(9)	1/4	0.5288(9)	1
S	2*e*	0.6494(10)	1/4	0.1947(7)	1
O1	4*f*	0.6963(11)	0.0921(8)	0.3111(8)	1
O2	2*e*	0.8304(17)	1/4	0.0729(13)	1
O3	2*e*	0.4007(18)	1/4	0.0413(12)	1
H1	4*f*	0.20500	0.58200	0.15400	1
H2	4*f*	0.09200	0.04500	0.20400	1
O4	4*f*	0.1579(10)	0.5462(7)	0.2183(8)	1

Table 3. Selected Bond Distances and Angles in $NaCoSO_4F \cdot 2H_2O$, $NaNiSO_4F \cdot 2H_2O$, and $NaFeSO_4F \cdot 2H_2O$

	$NaCoSO_4F \cdot 2H_2O$	$NaNiSO_4F \cdot 2H_2O$	$NaFeSO_4F \cdot 2H_2O$
	angles (deg)		
O4−Na−O4	78.4	76.43	75.7
O4−Na−O3	89.05	87.53	90.1
F−Na−O4	137.43	138.74	139.6
F−Na−O3	109.36	110.07	105.2
	distances (Å)		
Na−O4 (×2)	2.38	2.43	2.45
Na−F	2.27	2.22	2.34
Na−O3	2.34	2.36	2.31

two others (labeled O1) are sharing vertices of SO_4 tetrahedrons forming chains along the *b* axis (see Figure 2b). Looking closely to the structure, we noticed that these chains are interconnected, thanks to strongly distorted NaO_3F tetrahedrons (see Table 3 for selected angles and distances). Each NaO_3F tetrahedron is connected to three different chains by sharing two oxygen atoms (labeled O4, from the H_2O molecule) from two different MO_4F_2 octahedrons of the first chain, one fluorine atom from the neighboring MO_4F_2 chain, and finally, the third oxygen atom (labeled O3) is common to a SO_4 tetrahedron from the last chain (Figure 2b).

Thermal Stability. Thermogravimetric analyses coupled with mass spectrometry was performed in order to assess both the thermal stability of the samples and the water departure temperature. Alumina crucibles were loaded with 10−20 mg of powder sample and the experiments were run between 30 and 400 °C under a constant flow of dry argon (50 mL/min) using a simultaneous thermal analyzer STA 449C Jupiter from Netzsch and a heating/cooling rate of 10 °C/min. The released gases were analyzed by a quadrupole QMS 403 Aëolos mass spectrometer. For M = Co, we note a 14% weight loss in air occurring near 220 °C (Figure 3a) corresponding to the departure of water as confirmed by Mass Spectrometry. Such a weight loss corresponds to the departure of 2 water molecules per unit formula confirming further the material formula $NaCoSO_4F \cdot 2H_2O$ as deduced by XRD measurements. To test this hypothesis and obtain further insight into the thermal stability of the sample, we took temperature-controlled X-ray diffraction measurements on $NaCoSO_4F \cdot 2H_2O$ powders in air up to 600 °C. The same Bruker D8 diffractometer as above, but equipped with a HTK 1200 °C Anton Parr Chamber, was used to perform such measurements. Each pattern was recorded

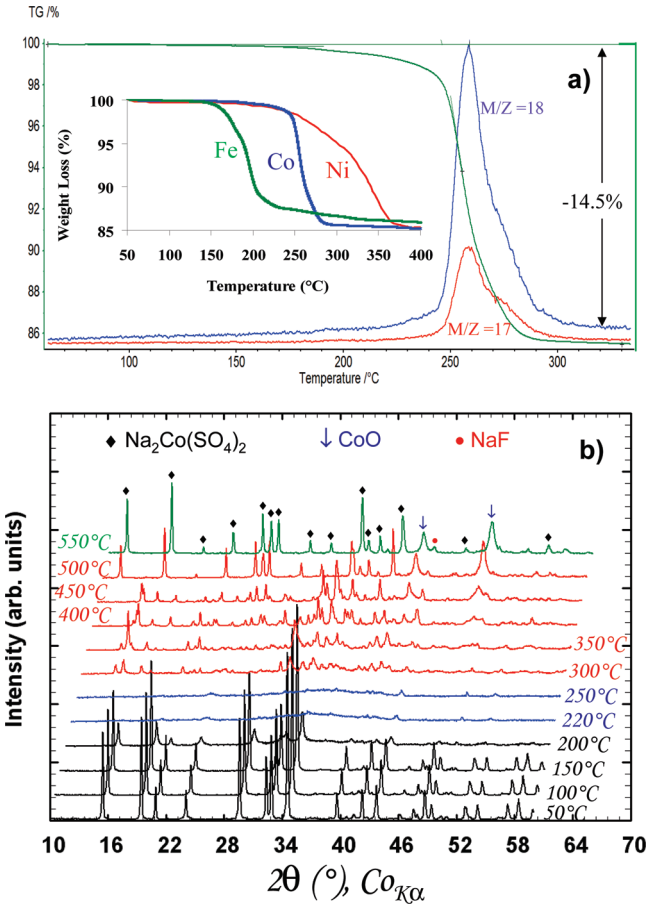

Figure 3. (a) Coupled TGA and mass spectrometry measurements of $NaCoSO_4F.2H_2O$ phases at a rate of 10 °C/min under air. The counting time for MS is of 20 ms per *m*/*z* values with a resting time of 1 s. *m*/*z* values of 17 and 18, corresponding to H_2O and OH species, respectively, were found. Needless to say, the presence of the "OH" gas is most likely the result of fragmentation in the mass spectrometer. The TGA curves for the M = Co, Ni and Fe phase are reported as inset. (b) Temperature-controlled X-ray diffraction ($\lambda_{Co-K\alpha}$) of $NaCoSO_4F \cdot 2H_2O$ showing amorphization for temperatures near 220 °C and the appearance of extra peaks different from those corresponding to $NaCoSO_4F$ for $T > 300$ °C.

for approximately 40 min at a constant temperature between $2\theta = 10°$ and $2\theta = 60°$. All collected XRD patterns (Figure 3b) remained alike until 200 °C, at this temperature the X-ray powder pattern becomes featureless, suggesting an amorphization of the material associated to the departure of water. Then upon further heating, few extra peaks began appearing and continued to grow (or the material further transformed) up to 400 °C. From data matching, we deduced that $NaCoSO_4F \cdot 2H_2O$ undergoes a non reversible dehydration process which leads to the formation of several phases with the main ones being $Na_2Co(SO_4)_2 + CoO + NaF$ at 500 °C. Whatever be the nature of M, we found that water removal does occur over the 200−380 °C range (Figure 3a inset), the highest water departure temperature being found when M = Ni ($T \approx 300$ °C).

Ionic liquids were recently shown within the $FeSO_4 \cdot nH_2O$ system to act as a mild dehydration agent enabling the control stabilization of the $n = 1$ ($FeSO_4 \cdot H_2O$) and $n = 0$ ($FeSO_4$) phases at $T = 90$ and 250 °C, respectively. We implemented this approach to the dehydration of $NaCoSO_4F \cdot 2H_2O$ and found by annealing the hydrated phase into an ionic liquid media (EMI-TFSI) at 260 °C for 2 h, the feasibility to obtain fully dehydrated $NaCoSO_4F$ (Figure 4a) having lattice parameters identical to those obtained when such a phase was prepared either by ionic liquid or ceramic processes enlisting the reaction of $CoSO_4 \cdot H_2O + NaF$.[16] It was noted that during such a process, the water does not escape but rather remains within the ionic liquid as an increase from 18 to 8000 ppm was deduced from Karl Fischer measurements. This finding led us to think of the removed water as being linked to the ionic liquid ions. Using a similar procedure, we could prepare the dehydrated version of the $NaFeSO_4F \cdot 2H_2O$ fluorosulphate bihydrate as well. In contrast, we could not succeed in obtaining the $NaNiSO_4F$. This does not come as a total surprise because the thermal stability of $NaNiSO_4F$ is known to be lower ($T_{dec} \approx 250$ °C)[16] than the temperature needed to remove water from the bihydrated $NaNiSO_4F \cdot 2H_2O$ phase. Attempts to obtain the Fe- and Co-based dehydrated phase via heating their corresponding hydrated phase under the flow of argon, nitrogen, air or under vacuum have suggested the special role played by ionic liquids. Such a result calls for numerous questions regarding the dehydration mechanism path (e.g., topotactic vs phase degradation and reformation) and the state of the removed water within the ionic liquid (e.g., water-ionic liquid interactions). Temperature-controlled in situ NMR experiments have been presently designed to track both of these aspects.

Water Loss Mechanism. To grasp further insights on the dehydration mechanism, temperature-controlled X-ray diffraction measurements, in presence of ionic liquids, were conducted under an N_2 atmosphere using a similar HTK 1200 °C Anton Parr Chamber as above. To combat the ionic liquid absorption, we minimize the amount of ionic liquid use by solely wetting our powder so as to have an ionic liquid film around the particles. By doing so we were able, as opposed of working solely under N_2 ambient, to spot the structural transition that begins as early as

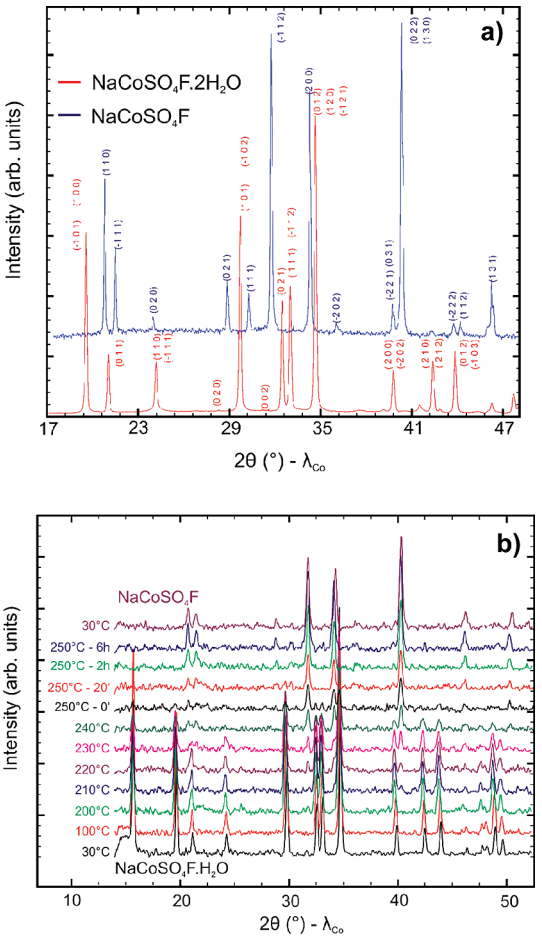

Figure 4. (a) XRD patterns of the $NaCoSO_4F \cdot 2H_2O$ phase and of the $NaCoSO_4F$ phase obtained by dehydration of the former in ionic liquid media. (b) Temperature-controlled X-ray diffraction ($\lambda_{Co-K\alpha}$) of $NaCoSO_4F \cdot 2H_2O$ in ionic liquid media showing the progressive transformation from the hydrated to the dehydrated $NaCoSO_4F$ phase.

210 °C (Figure 4b) with namely the appearance of two Bragg peaks at $2\theta \approx 32$ and 34°, reminiscent of $NaCoSO_4F$, which grow with increasing temperature. At 250 °C, the dehydration is completed and increasing the heating time simply results in a sharpening of the XRD pattern.

The dehydration process was further monitored by TEM. The pristine hydrated phase, final dehydrated compound, and intermediate samples were all observed. The starting material is composed of large monolithic particles (in the micrometer range) having a rectangular shape (Figure 5a). As soon as the dehydration starts, nucleation takes place at several sites on the crystals. Due to the strong decrease in the cell volume between hydrated ($V/Z \approx 138$ Å^3) and dehydrated ($V/Z \approx 93.5$ Å^3) phases, strains and breaks are observed within the particles (Figure 5b). Then, as the structure collapses according to the mechanism proposed below, we note a chemical grinding of the main particle leading to the formation of agglomerates made of 0.2−0.3 μm particles (Figure 5c). Therefore, the global rectangular shape of the initial particles seems to be preserved. Additionally, it is worth noting the large porosity for these agglomerates. The TEM study of the fully dehydrated phase (Figure 5d) shows that part of the mechanism implies a partial dissolution of the material since larger particles

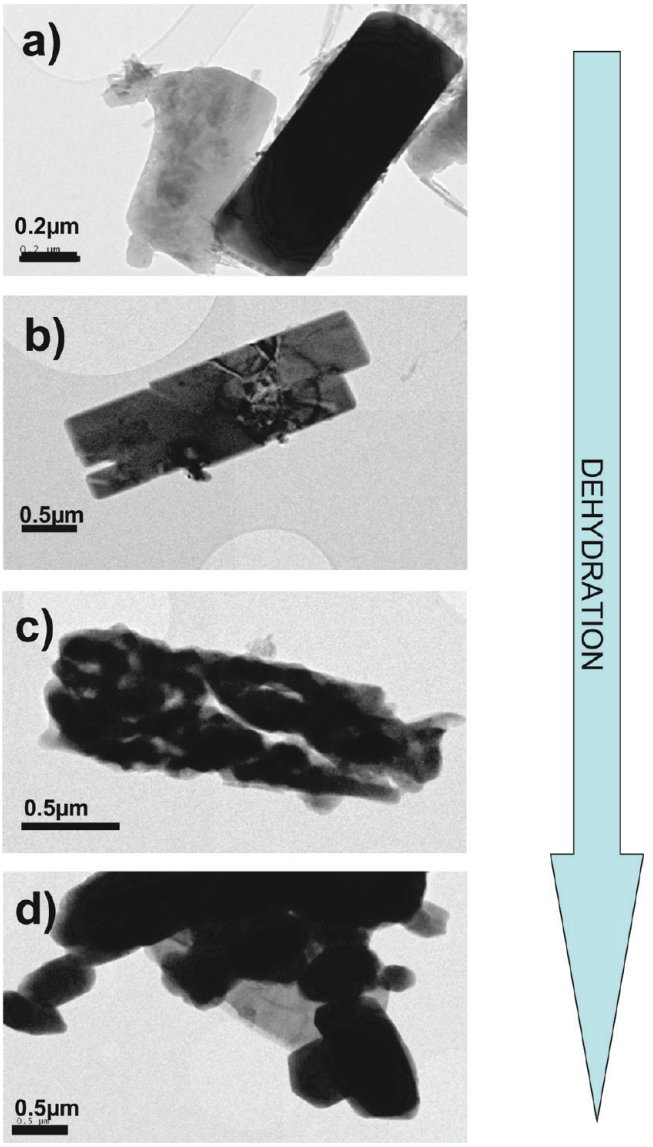

Figure 5. Evolution of the shape, size, and porosity of the particles of $NaMSO_4F \cdot 2H_2O$ (M = Fe, Co, Ni) during the dehydration process as observed by TEM: (a) pristine bihydrated phase, (b) nucleation of the new phase inducing strains, (c) collapse of the particles into small dehydrated particles, and (d) growth of the particles through a Ostwald-type ripening.

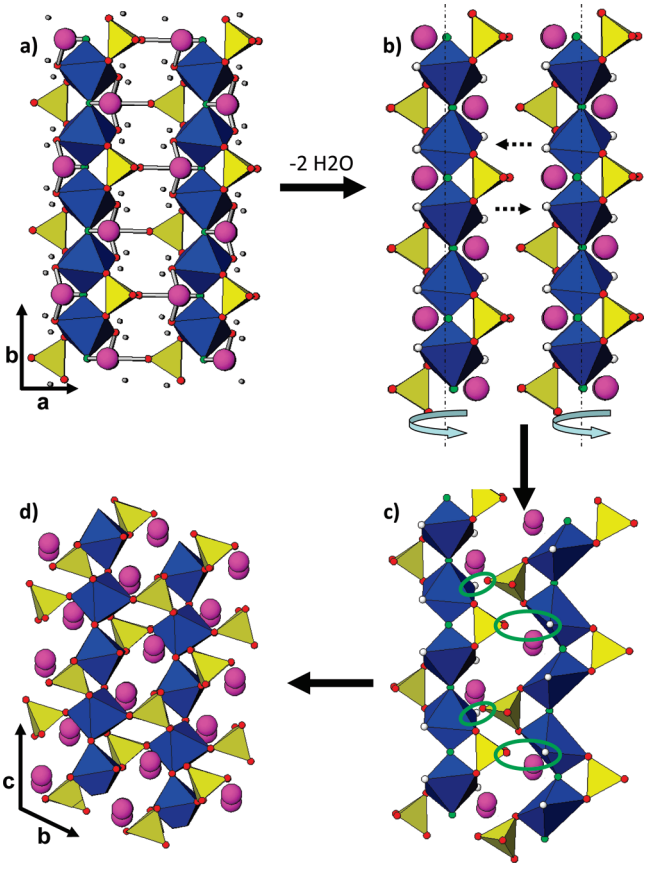

Figure 6. Comparative structural diagrams depicting the water removal mechanism from $NaMSO_4F \cdot 2H_2O$ to form $NaMSO_4F$: (a) initial $NaMSO_4F \cdot 2H_2O$, (b) dehydrated $NaMSO_4F$, (c) distortion of chains of octahedra and tetrahedra to form new bonds, and (d) the final $NaMSO_4F$ structure.

(0.6 μm) are observed at the end. It seems that a process somewhat related to Ostwald-type ripening with a partial dissolution and crystallization of the material does occur. This is consistent with the observed sharpening of the Bragg peaks when the material is aged at 250 °C.

From structural comparison of both bihydrated (Figure 6a) and dehydrated (Figure 6d) phases, a reaction mechanism could be proposed. The water departure from the hydrated phase induces a collapse of the structure (namely of the layers perpendicular to the $\vec{a}$ direction) with a rotation of the chains of octahedra and tetrahedra along an axis parallel to $\vec{b}$ (Figure 6b). Then, new bonds are formed between oxygen atoms at the edges of tetrahedra and the closest transition metal cation (from the following octahedra chain) to compensate the vacancies (white spheres on the figure) created by the water departure (Figure 6c). Thus a distortion and stretching of both octahedra and tetrahedra is necessary to finally obtain structure of the dehydrated phase.

Redox and Transport Properties. The electrochemical performance of some of these $NaMSO_4F.H_2O$ phases, ball-milled with 15% w/w carbon black (SP) for 15 min, were tested vs Li in both Li-and Na half-Swagelok cells with a special attention to the $NaFeSO_4F \cdot 2H_2O$ phase, which from comparative arguments should fall within the 3.5−4 V voltage range. The cells were assembled in an argon-filled glovebox, using a Na metal disk as the negative electrode, a Whatman GF/D borosilicate glass fiber sheet saturated with 1 M $NaClO_4$ in propylene carbonate (PC) as the electrolyte. Regardless of the nature of M (Fe, Co or Ni) and independent of whether the cell was initially reduced or oxidized, no reversible electrochemical activity was found. Similarly, no electrochemical activity was observed when the electrodes were cycled vs a Li metal disk negative electrode using 1 M $LiPF_6$ in ethylene carbonate (EC), dimethyl carbonate (DMC) (1:1 w/w) as the electrolyte. In an attempt to explain the absence of redox activity for these new transition metal (Fe, Co, Ni) sodium fluorosulphates, we have measured the ionic conductivities.

Conductivity values were measured for $NaCoSO_4F \cdot 2H_2O$ and its dehydrated version $NaCoSO_4F$. These powders were pressed into (green) dense pellets by first uniaxial pressing (500 kg·cm^2) followed by isostatic

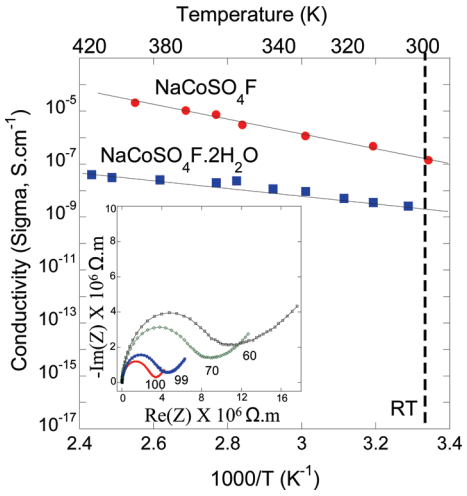

Figure 7. Conductivity of $NaCoSO_4F \cdot 2H_2O$ and its dehydrated analogue $NaCoSO_4F$ pellets at different temperature coated with ionically blocking Au electrodes. Inset, representative AC impedance spectra (Nyquist plot) of $NaCoSO_4F \cdot 2H_2O$ pellet. They have a slightly depressed high-frequency semicircle and a low-frequency Warburg diffusion line. The equivalent circuit consists of a resistance and a capacitance in parallel connection.

pressing (2500 bar). These pellets were annealed at 140 °C for 3 h under primary vacuum to ensure complete removal of any surface-adsorbed water, while retaining the primary phase. Next, gold was sputtered on both faces of the pellet in order to form ionically blocking electrodes. AC and DC conductivity was measured by employing (ac) impedance spectroscopy (200 kHz to 10 mHz) and 1 V d.c. polarization (that is below the decomposition potential) at different temperatures (RT−140 °C) using Bio-Logic VMP3 unit. Typical impedance spectra suggest ionic nature of a.c. conductivity, consisting of a depressed semicircle (at high frequency) along with a Warburg diffusion line (at low frequency) (Figure 7, inset). The ac conductivity value of $NaCoSO_4F \cdot 2H_2O$ was found to be 2.43×10^{-9} S cm^{-1} at ambient temperature (Figure 7), which is lower than $NaCoSO_4F$ conductivity of 1.46×10^{-7} S cm^{-1}. The activation energy (E_{ac}) values for $NaCoSO_4F \cdot 2H_2O$ and $NaCoSO_4F$ were 0.619 ± 0.01 eV and 0.438 ± 0.03 eV, respectively. The DC conductivity values for $NaCoSO_4F.2H_2O$ and $NaCoSO_4F$ were 1.85×10^{-10} S m^{-1} ($E_{ac} = 0.619 \pm 0.03$ eV) and 9.5×10^{-11} S cm^{-1} ($E_{ac} = 0.633 \pm 0.02$ eV), respectively. These monoclinic-structured Na-based compounds have a rigid interconnected $MO_4F_2-SO_4$ framework, which facilitates high ionic transport.[16] At this stage, the effect of structural water and relative contribution from Na^+, H^+, and possibly F^- is being investigated combining NMR diffusion measurements and first-principle calculations under the DFT + U framework.

Discussion and Conclusions

In summary, via the use of a low-temperature process enlisting the dissolution of a 3*d*-metal hydrate sulphates and NaF precursors in aqueous media, we succeeded in preparing a new class of Na-based 3d metal fluorosulphate hydrates. Among these new compounds, the Fe phase was found to be the most difficult to obtain because of the tendency of Fe^{2+} to oxidize to Fe^{3+} in an oxygen containing environment. In contrast, the Na-based Cobalt fluorosulphate hydrate phase was the easiest one to obtain. In addition to recrystallization in alcohol, it is possible to obtain a pure Co-based phase by slowly evaporating water at 70 °C over the course of several days. Reaction temperature and precursor concentration was found to govern the obtention of these bihydrated fluorosulphate phases. Thermodynamic calculations are presently underway to determine the role of temperature, precursor concentration and pH so as to provide guidance for implementing this approach toward a wider class of fluorosulphate materials. Replacing NaF by other alkali halogenide salts (MX; M = Li, Na, K and X = F, Cl, OH) was also shown to lead to a few halogenide sulfate hydrate phases to be reported in a forthcoming paper, with the most difficulties encountered for M = Li because of the poor solubility of LiF in aqueous media (e.g., 3 g per liter).

The ability to stabilize the $NaMSO_4F$ phases having a tavorite-like structure upon dehydration of the new fluorosulphate bihydrate phases came as a pleasant surprise because such $NaMSO_4F$ (M = Fe, Co, and Ni) are by themselves soluble in aqueous media. Upon such a dehydration process, the vacancies created by the water departure are compensated by oxygen from the SO_4 tetrahedra via the formation of M−O−S bonding, leading to the dehydrated phase having a tavorite-type structure with chains along the *c*-axis bridged by isolated SO_4 tetrahedra. Such a complex structural mechanism, enlisting a drastic reorganization of the structure, is kinetically limited. This is consistent with the experimental observation that any tentative dehydration experiments conducted under various gas flowing processes or vacuum have failed as opposed to the dehydration in the ionic liquid media, which provides a kinetic lag in the water departure process. To further shed some light on this water departure−structural reorganization mechanism, in situ NMR experiments are presently underway.

Turning to the transport properties, the lower ionic conductivity for the bihydrated phase as compared to the dehydrated one can be explained from structural considerations. Indeed, in both phases, sodium ions are coordinated to 3 oxygens and 1 fluorine. But although in the dehydrated phase Na ions are sitting in a quasi-planar environment, they are located into disordered tetrahedrons in the hydrated compounds, implying a limited mobility. Last, the present synthetic approach offers an indirect method to prepare the Li-based fluorosulphates that we are presently exploiting so as to widen the members of this fluorosulphate family that was still unknown 1 year ago.

Acknowledgment. We thank M. Courty for performing some of the TGA measurements, T. Bataille for insightful discussions regarding sulphate chemistry, M. Reynaud for characterizing some of the reported materials, and C. Delacourt for his help regarding the AC/DC conductivity measurements.